

Cloud Quantum Computing of an Atomic Nucleus*

E. F. Dumitrescu,¹ A. J. McCaskey,² G. Hagen,^{3,4} G. R. Jansen,^{5,3} T. D. Morris,^{4,3}
T. Papenbrock,^{4,3,†} R. C. Pooser,^{1,4} D. J. Dean,³ and P. Lougovski^{1,‡}

¹*Computational Sciences and Engineering Division,
Oak Ridge National Laboratory, Oak Ridge, TN 37831, USA*

²*Computer Science and Mathematics Division, Oak Ridge National Laboratory, Oak Ridge, TN 37831, USA*

³*Physics Division, Oak Ridge National Laboratory, Oak Ridge, TN 37831, USA*

⁴*Department of Physics and Astronomy, University of Tennessee, Knoxville, TN 37996, USA*

⁵*National Center for Computational Sciences, Oak Ridge National Laboratory, Oak Ridge, TN 37831, USA*

We report a quantum simulation of the deuteron binding energy on quantum processors accessed via cloud servers. We use a Hamiltonian from pionless effective field theory at leading order. We design a low-depth version of the unitary coupled-cluster ansatz, use the variational quantum eigensolver algorithm, and compute the binding energy to within a few percent. Our work is the first step towards scalable nuclear structure computations on a quantum processor via the cloud, and it sheds light on how to map scientific computing applications onto nascent quantum devices.

Introduction.—Solving the quantum many-body problem remains one of the key challenges in physics. For example, wavefunction-based methods in nuclear physics [1–3] face the exponential growth of Hilbert space with increasing number of nucleons, while quantum Monte Carlo methods [4–6] are confronted with the fermion sign problem [7]. Quantum computers promise to reduce the computational complexity of simulating quantum many-body systems from exponential to polynomial [8]. For instance, a quantum computer with about 100 error-corrected qubits could potentially revolutionize nuclear shell-model computations. However, present quantum devices are limited to about 20 non-error corrected qubits, and the implementation of quantum many-body simulation algorithms on these devices faces gate and measurement errors, and qubit decoherence. Nonetheless, the outlook for quantum simulations is promising. A body of cutting edge research is aimed at reducing computational complexity of quantum simulation algorithms to match algorithmic requirements to the faulty hardware [9].

Recently, real-world problems in quantum chemistry and magnetism have been solved via quantum computing using two to six qubits [10–13]. These ground-breaking quantum computing experiments used phase estimation algorithms [14] and the variational quantum eigensolver

(VQE) [11, 15]. They were performed by a few teams of hardware developers working alongside theorists. However, the field of quantum computing has now reached a stage where a remote computation can be performed with minimal knowledge of the hardware architecture. Furthermore, the relevant software (e.g. PyQuil [16], XACC [17], OpenQASM [18], and OpenFermion [19]) to run on quantum computers and simulators is publicly available. Cloud access and cloud service to several quantum processors now allows the broader scientific community to explore the potential of quantum computing devices and algorithms.

In this Letter we present a quantum computation of the deuteron, the bound state of a proton and a neutron, and we use only publicly available software and cloud quantum hardware (IBM Q Experience and Rigetti 19Q [20]). The problem of quantum computing the deuteron binding energy is still non-trivial because we have to adjust the employed Hamiltonian, the wavefunction preparation, and the computational approach to the existing realities of cloud quantum computing. For example, the limited connectivity between qubits on a quantum chip, the low depth (the number of sequential gates) of quantum circuits due to decoherence, a limited number of measurements via the cloud, and the intermittent cloud access in a scheduled environment must all be taken into account.

This Letter is organized as follows. First, we introduce and tailor a deuteron Hamiltonian from pionless effective field theory (EFT) such that it can be simulated on a quantum chip. Next, we introduce a variational wavefunction ansatz based on unitary coupled-cluster theory (UCC) [15, 21] and reduce the circuit depth, and the number of two-qubit entangling operations, such that all circuit operations can be performed within the device’s decoherence time. Next, we present the results of our cloud quantum computations, performed on IBM QX5 and Rigetti 19Q quantum chips. Finally we give a summary and an outlook.

* This manuscript has been authored by UT-Battelle, LLC under Contract No. DE-AC05-00OR22725 with the U.S. Department of Energy. The United States Government retains and the publisher, by accepting the article for publication, acknowledges that the United States Government retains a non-exclusive, paid-up, irrevocable, world-wide license to publish or reproduce the published form of this manuscript, or allow others to do so, for United States Government purposes. The Department of Energy will provide public access to these results of federally sponsored research in accordance with the DOE Public Access Plan. (<http://energy.gov/downloads/doe-public-access-plan>).

† Corresponding author: tpapenbr@utk.edu

‡ email: lougovskip@ornl.gov

Hamiltonian and model space.—Pionless EFT provides a systematically improvable and model-independent approach to nuclear interactions in a regime where the momentum scale Q of the interesting physics is much smaller than a high-momentum cutoff Λ [22, 23]. At leading order, this EFT describes the deuteron via a short-ranged contact interaction in the 3S_1 partial wave. We follow Refs. [24, 25] and use a discrete variable representation in the harmonic oscillator basis for the Hamiltonian. The deuteron Hamiltonian is

$$H_N = \sum_{n,n'=0}^{N-1} \langle n'|(T+V)|n\rangle a_n^\dagger a_n. \quad (1)$$

Here, the operators a_n^\dagger and a_n create and annihilate a deuteron in the harmonic-oscillator s -wave state $|n\rangle$. The matrix elements of the kinetic and potential energy are

$$\begin{aligned} \langle n'|T|n\rangle &= \frac{\hbar\omega}{2} \left[(2n+3/2)\delta_n^{n'} - \sqrt{n(n+1/2)}\delta_n^{n'+1} \right. \\ &\quad \left. - \sqrt{(n+1)(n+3/2)}\delta_n^{n'-1} \right], \\ \langle n'|V|n\rangle &= V_0\delta_n^0\delta_n^{n'}. \end{aligned} \quad (2)$$

Here, $V_0 = -5.68658111$ MeV, and $n, n' = 0, 1, \dots, N-1$, for a basis of dimension N . We set $\hbar\omega = 7$ MeV, and the potential has an ultraviolet cutoff $\Lambda \approx 152$ MeV [26], which is still well separated from the bound-state momentum of about $Q \approx 46$ MeV.

Mapping the deuteron onto qubits.—Quantum computers manipulate qubits by operations based on Pauli matrices (denoted as X_q , Y_q , and Z_q on qubit q). The deuteron creation and annihilation operators can be mapped onto Pauli matrices via the Jordan-Wigner transformation

$$\begin{aligned} a_n^\dagger &\rightarrow \frac{1}{2} \left[\prod_{j=0}^{n-1} -Z_j \right] (X_n - iY_n), \\ a_n &\rightarrow \frac{1}{2} \left[\prod_{j=0}^{n-1} -Z_j \right] (X_n + iY_n). \end{aligned} \quad (3)$$

A spin up $|\uparrow\rangle$ (down $|\downarrow\rangle$) on qubit n corresponds to zero (one) deuteron in the state $|n\rangle$. As we deal with single-particle states, the symmetry under permutations plays no role here. To compute the ground-state energy of the deuteron we employ the following strategy. We determine the ground-state energies of the Hamiltonian (1) for $N = 1, 2, 3$ and use those values to extrapolate the energy to the infinite-dimensional space. We have $H_1 = 0.218291(Z_0 - I)$ MeV, and its ground-state energy $E_1 = \langle \downarrow|H_1|\downarrow\rangle \approx -0.436$ MeV requires no computation. Here, I denotes the identity operation. For

E from exact diagonalization				
N	E_N	$\mathcal{O}(e^{-2kL})$	$\mathcal{O}(kLe^{-4kL})$	$\mathcal{O}(e^{-4kL})$
2	-1.749	-2.39	-2.19	
3	-2.046	-2.33	-2.20	-2.21
E from quantum computing				
N	E_N	$\mathcal{O}(e^{-2kL})$	$\mathcal{O}(kLe^{-4kL})$	$\mathcal{O}(e^{-4kL})$
2	-1.74(3)	-2.38(4)	-2.18(3)	
3	-2.08(3)	-2.35(2)	-2.21(3)	-2.28(3)

TABLE I. Ground-state energies of the deuteron (in MeV) from finite-basis calculations (E_N) and extrapolations to infinite basis size at a given order of the extrapolation formula (6). The upper part shows results from exact diagonalizations in Hilbert spaces with N single-particle states, and the lower part the results from quantum computing on N qubits. We have $E_1 = -0.436$ MeV. The fit at $\mathcal{O}(e^{-4kL})$ requires three parameters and is only possible for $N = 3$. The deuteron ground-state energy is -2.22 MeV.

$N = 2, 3$ we have (all numbers are in units of MeV)

$$H_2 = 5.906709I + 0.218291Z_0 - 6.125Z_1 - 2.143304(X_0X_1 + Y_0Y_1), \quad (4)$$

$$H_3 = H_2 + 9.625(I - Z_2) - 3.913119(X_1X_2 + Y_1Y_2). \quad (5)$$

For the extrapolation to the infinite space we employ the harmonic-oscillator variant of Lüscher's formula [27] for finite-size corrections to the ground-state energy [28]

$$\begin{aligned} E_N &= -\frac{\hbar^2k^2}{2m} \left(1 - 2\frac{\gamma^2}{k}e^{-2kL} - 4\frac{\gamma^4L}{k}e^{-4kL} \right) \\ &\quad + \frac{\hbar^2k\gamma^2}{m} \left(1 - \frac{\gamma^2}{k} - \frac{\gamma^4}{4k^2} + 2w_2k\gamma^4 \right) e^{-4kL}. \end{aligned} \quad (6)$$

Here, the finite-basis result E_N equals the infinite-basis energy $E_\infty = -\hbar^2k^2/(2m)$ plus exponentially small corrections. In Eq. (6), $L = L(N)$ is the effective hard-wall radius for the finite basis of dimension N , k is the bound-state momentum, γ the asymptotic normalization coefficient, and w_2 an effective range parameter. For $N = 1, 2$ and 3 we have $L(N) = 9.14, 11.45$, and 13.38 fm as the effective hard-wall radius in the oscillator basis with $\hbar\omega = 7$ MeV, respectively, and $L(N) \approx \sqrt{(4N+7)\hbar/(m\omega)}$ for $N \gg 1$ [29]. Using the ground-state energies E_N for $N = 1, 2$ allows one to fit the leading $\mathcal{O}(e^{-2kL})$ and subleading $\mathcal{O}(kLe^{-4kL})$ corrections by adjusting k and γ . Inclusion of the $N = 3$ ground-state energy also allows one to fit the smaller $\mathcal{O}(e^{-4kL})$ correction by adjusting w_2 . The results of this extrapolation are presented in the upper part of Table I, together with the energies E_N from matrix diagonalization. We note that the most precise $N = 2$ ($N = 3$) extrapolated result is about 2% (0.5%) away from the deuteron's ground-state energy of -2.22 MeV.

Variational wavefunction.—In quantum computing, a popular approach to determine the ground-state energy

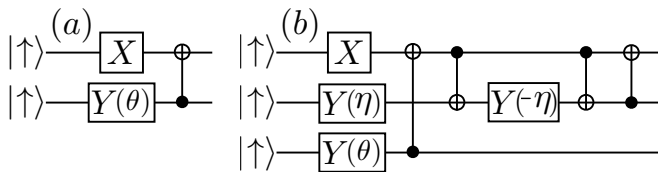


FIG. 1. Low-depth circuits that generate unitary rotations in Eq. (7) (panel a) and Eq. (8) (panel b). Also shown are the single-qubit gates of the Pauli X matrix, the rotation $Y(\theta)$ with angle θ around the Y axis, and the two-qubit CNOT gates.

of a Hamiltonian is to use UCC ansatz in tandem with the VQE algorithm [12, 15, 21]. We adopt this strategy for the Hamiltonians described by Eqs. (4) and (5). We define unitary operators entangling two and three orbitals,

$$U(\theta) \equiv e^{\theta(a_0^\dagger a_1 - a_1^\dagger a_0)} = e^{i\frac{\theta}{2}(X_0 Y_1 - X_1 Y_0)}, \quad (7)$$

$$U(\eta, \theta) \equiv e^{\eta(a_0^\dagger a_1 - a_1^\dagger a_0) + \theta(a_0^\dagger a_2 - a_2^\dagger a_0)} \quad (8) \\ \approx e^{i\frac{\eta}{2}(X_0 Y_1 - X_1 Y_0)} e^{i\frac{\theta}{2}(X_0 Z_1 Y_2 - X_2 Z_1 Y_0)}.$$

In the second line of Eq. (8) we expressed the exponential of the sum as the product of exponentials and note that the discarded higher order commutators act trivially on the initial product state $|\downarrow\uparrow\uparrow\rangle$. We seek an implementation of these unitary operations in a low-depth quantum circuit. We note that $U(\eta)$ and $U(\eta, \theta)$ can be simplified further because a single-qubit rotation about the Y axis implements the same rotation as Eq. (7) within the two-dimensional subspace $\{|\downarrow\uparrow\uparrow\rangle, |\uparrow\downarrow\uparrow\rangle\}$. Likewise Eq. (8) can be simplified by the above argument except the first rotation now lies within the $\{|\downarrow\uparrow\uparrow\rangle, |\uparrow\downarrow\uparrow\rangle\}$ subspace. The second rotation, acting within the $\{|\downarrow\uparrow\uparrow\rangle, |\uparrow\downarrow\uparrow\rangle\}$ subspace, must be implemented as a Y -rotation controlled by the state of qubit 0 in order to leave the $|\uparrow\downarrow\uparrow\rangle$ component unmodified. The resulting gate decomposition for the UCC operations are illustrated in Fig. 1.

Quantum computation.—We use the VQE [11] quantum-classical hybrid algorithm to minimize the Hamiltonian expectation value for our wavefunction ansatz. In this approach, the Hamiltonian expectation value is directly evaluated on a quantum processor with respect to a variational wavefunction, i.e. the expectation value of each Pauli term appearing in the Hamiltonian is measured on the quantum chip. We recall that quantum-mechanical measurements are stochastic even for an isolated system, and that noise enters through undesired couplings with the environment. To manage noise, we took the maximum of 8,192 (10,000) measurements that were allowed in cloud access for each expectation value on the QX5 (19Q) quantum device. In contrast, the recent experiment [13] by the IBM group employed up to 10^5 measurements and estimated that 10^6 would be necessary to reach chemical accuracy on the six-qubit realization of the BeH_2 molecule involving more than a hundred

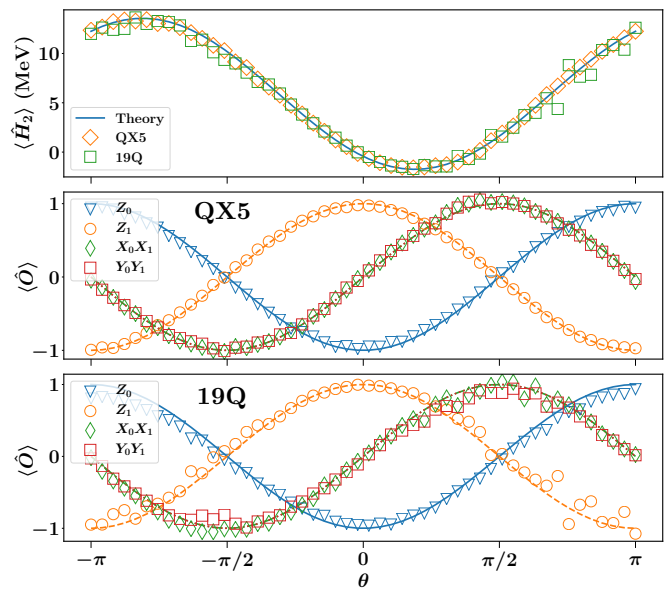


FIG. 2. (Color online) Experimentally determined energies for H_2 (top) and expectation values of the Pauli terms that enter the two-qubit Hamiltonian H_2 as determined on the QX5 (center) and 19Q (bottom) chips. Experimental (theoretical) results are denoted by symbols (lines).

Pauli terms. In addition to statistical errors, we address systematic measurement errors by shifting and re-scaling experimental expectation values as outlined in the supplemental material of Ref. [13]. The expectation values returned from the quantum device are then used on a classical computer to find the optimal rotation angle(s) that minimize the energy, or the parametric dependence of the energy on the variational parameters is mapped for the determination of the minimum [12].

Our results are based on cloud access to the QX5 and the 19Q chips, which consist of 16 and 19 superconducting qubits, respectively, with a single qubit connected to up to three neighbors. This layout is well suited for our task, because the Hamiltonian (5) only requires up to two connections for each qubit. We collected extensively more data on the QX5 device than on the 19Q and only ran the $N = 2$ problem on the latter.

Results.—Figure 2 shows $\langle H_2 \rangle$ (top panel) and the expectation values of the four Pauli terms that enter the Hamiltonian H_2 as a function of the variational parameter θ for the QX5 (center panel) and the 19Q (bottom panel). We see that the measurements are close to the exact results, particularly in the vicinity of the variational minimum of the energy. Cloud access, and its occasional network interruptions, made the direct minimization of the energy surface via VQE very challenging. Instead, we determined the minimum energies $E_2^{\text{QX5}} \approx -1.80 \pm 0.05$ MeV and $E_2^{19\text{Q}} \approx -1.72 \pm 0.03$ MeV from fitting a cubic spline close to the respective minimum.

Overall, the results obtained with the QX5 and 19Q quantum chips are comparable in quality, keeping in mind the much larger access times we had on the former device. Combining the independent results on both chips yields $E_2 = -1.74 \pm 0.03$ MeV. This energy, as well as the individual results, agree with the exact energy of -1.749 MeV within uncertainties, see Table I.

To obtain the infinite-space result, we apply the leading and subleading terms of the extrapolation formula Eq. (6) to our energies, i.e. $E_1 = -0.436$ MeV and $E_2 = -1.74 \pm 0.03$ MeV, and adjust k and γ . The results for the extrapolated energy $E_\infty = -\hbar^2 k^2 / (2m)$ are presented in Table I at leading and subleading order of the extrapolation. They agree within uncertainties with those from the exact diagonalization. Additionally, the $\mathcal{O}(kLe^{-4kL})$ result of $-2.18(3)$ MeV deviates less than 2% from the exact deuteron ground-state energy of -2.22 MeV.

As a consistency check, we turn our attention to the $N = 3$ case. These quantum computations were only performed on the QX5. We optimized two angles to find the minimum energy of the Hamiltonian in Eq. (5). We performed the minimization by choosing grids with increasingly fine spacing in the parameter space around the minimum (initially coarsely sampling the entire parameter space), computed the energy expectation values on the quantum device, and determined the minimum by a fit to cubic splines. This minimization problem is significantly more challenging than for the $N = 2$ case because the increased number of CNOT gates introduced more noise and errors.

In addition to correcting assignment errors, we implemented the zero-noise extrapolation hybrid quantum-classical error mitigation techniques [30]. For the zero-noise extrapolation, we extrapolated the Hamiltonian expectation values $\langle \hat{O} \rangle$ to their noiseless limit $\langle \hat{O} \rangle(0)$ with respect to noise induced by the two-qubit CNOT operations. Since the true entangler error model is not well established, we assume that a generic two-qubit white noise error channel $\mathcal{E}(\rho) = (1 - \varepsilon)\rho + \varepsilon I/4$, where ρ denotes the density matrix, follows the application of each CNOT. We then artificially increased the error rate ε by adding pairs of CNOT gates (i.e. noisy identity gates) to each CNOT appearing in our original circuit. Our overall noise model is thus parameterized by $r\varepsilon$, where r is the number of CNOT gate repetitions. A set of noisy expectation values $\langle \hat{O} \rangle(r)$ are experimentally determined and used to estimate their noiseless counterpart $\langle \hat{O} \rangle(0)$ [30]. Kraus decomposing the white noise channel in the two-qubit Pauli basis and noting that CNOT maps the Pauli group onto itself, one can see that the noise channel commutes and CNOT operators commute. After applying r CNOTs (denoted by the operator CX), the noise channel becomes $\mathcal{E}_r(\rho) = (1 - r\varepsilon)CX\rho CX + r\varepsilon I/4 + \mathcal{O}(\varepsilon^2)$. Given the small CNOT error rate, quadratic contributions may be discarded and a linear regression of the form

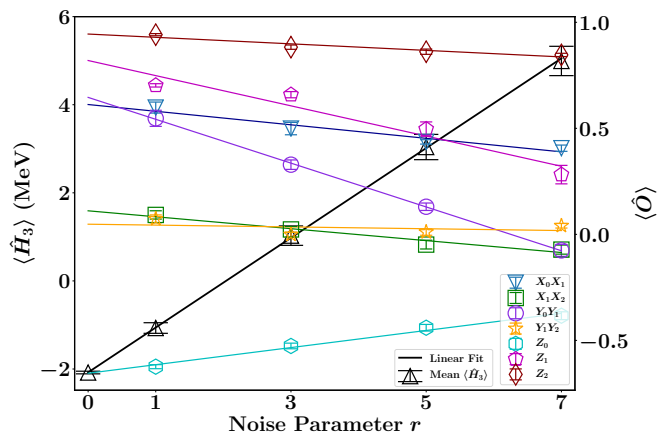


FIG. 3. (Color online) Noise extrapolation of the $N = 3$ qubit problem run on the QX5. The H_3 energy (left axis, black line) and individual Pauli expectation values (right axis) are given as a function of the number CNOT gate scaling factor r .

$\langle \hat{O} \rangle(r) = \langle \hat{O} \rangle(0) + \chi r$, with the slope $\chi = -\langle \hat{O} \rangle(0)\varepsilon$ yields noiseless expectation values. Computing the individual Hamiltonian expectation values for $r = 1, 3, 5, 7$ using ten iterations of 8,192 measurements, we then linearly extrapolated to the noiseless limit of $r = 0$. This approach yields a minimum energy $E_3 = -2.08 \pm 0.03$ MeV and agrees with the exact result within uncertainties. Figure 3 shows the details of the noise extrapolations.

Finally, we include the $N = 3$ results and apply the extrapolation (6) to find the infinite-space energy. The results are shown in the lower part of Table I. We see that the extrapolated energies agree with the exact results at the lowest two orders. For the $\mathcal{O}(e^{-4kL})$ extrapolation, however, the extrapolated energy yields about 3% too much binding, and this reflects the differences between the E_3 value from the exact and the quantum computation.

Summary.—We performed a quantum computation of the deuteron binding energy via cloud access to two quantum devices. The Hamiltonian was taken from pionless effective field theory at leading order, and we employed a discrete variable representation to match its structure to the connectivity of the available hardware. We adapted the circuit depth of the state preparation to the constraints imposed by the fidelity of the devices. The results from our two-qubit computations on the IBM QX5 and the Rigetti 19Q devices agree with each other and with the exact result within our small (a few percent) uncertainties; the extrapolation to infinite Hilbert spaces yields a result within 2% percent of the deuteron’s binding energy. Employing a third qubit makes the computation more challenging due to entanglement errors. Error correction methods again yield a deuteron energy that agrees with exact results within uncertainties. The extrapolation to infinite space is within 3% of the exact result. The presented results open the avenue for quan-

tum computations of heavier nuclei via cloud access.

We acknowledge access to the IBM QX5 quantum chip, the Rigetti Quantum Virtual Machine, and to the Rigetti 19Q quantum chip. Plots were made with Matplotlib [31]. This material is based upon work supported by the U.S. Department of Energy, Office of Science, Office of Nuclear Physics, under grants DE-FG02-96ER40963, de-sc0018223 (NUCLEI SciDAC-4 collaboration), and the field work proposals ERKBP57 and ERKBP72 at Oak Ridge National Laboratory (ORNL). This material is based upon work supported by the U.S. Department of Energy, Office of Science, Office of Advanced Scientific Computing Research (ASCR) quantum algorithms and testbed programs, under field work proposal numbers ERKJ332 and ERKJ335. This work used resources of the Oak Ridge Leadership Computing Facility located at ORNL, which is supported by the Office of Science of the Department of Energy under Contract No. DE-AC05-00OR22725.

-
- [1] E. Caurier, G. Martínez-Pinedo, F. Nowacki, A. Poves, and A. P. Zuker, “The shell model as a unified view of nuclear structure,” *Rev. Mod. Phys.* **77**, 427–488 (2005).
- [2] P. Navrátil, S. Quaglioni, I. Stetcu, and B. R. Barrett, “Recent developments in no-core shell-model calculations,” *J. Phys. G* **36**, 083101 (2009).
- [3] B. R. Barrett, P. Navrátil, and J. P. Vary, “Ab initio no core shell model,” *Prog. Part. Nucl. Phys.* **69**, 131 – 181 (2013).
- [4] S. E. Koonin, D. J. Dean, and K. Langanke, “Shell model monte carlo methods,” *Physics Reports* **278**, 2 – 77 (1997).
- [5] Dean Lee, “Lattice simulations for few- and many-body systems,” *Progress in Particle and Nuclear Physics* **63**, 117 – 154 (2009).
- [6] J. Carlson, S. Gandolfi, F. Pederiva, Steven C. Pieper, R. Schiavilla, K. E. Schmidt, and R. B. Wiringa, “Quantum monte carlo methods for nuclear physics,” *Rev. Mod. Phys.* **87**, 1067–1118 (2015).
- [7] M. Troyer and U. Wiese, “Computational Complexity and Fundamental Limitations to Fermionic Quantum Monte Carlo Simulations,” *Physical Review Letters* **94**, 170201–170201 (2005).
- [8] M.A. Nielsen and I.L. Chuang, *Quantum Computation and Quantum Information: 10th Anniversary Edition* (Cambridge University Press, 2010).
- [9] R. Babbush, N. Wiebe, J. McClean, J. McClain, H. Neven, and G. Kin-Lic Chan, “Low Depth Quantum Simulation of Electronic Structure,” *ArXiv e-prints* (2017), arXiv:1706.00023 [quant-ph].
- [10] B. P. Lanyon, J. D. Whitfield, G. G. Gillett, M. E. Goggin, M. P. Almeida, I. Kassal, J. D. Biamonte, M. Mohseni, B. J. Powell, M. Barbieri, A. Aspuru-Guzik, and A. G. White, “Towards quantum chemistry on a quantum computer,” *Nature Chemistry* **2**, 106 (2010).
- [11] A. Peruzzo, J. McClean, P. Shadbolt, M.-H. Yung, X.-Q. Zhou, P. J. Love, A. Aspuru-Guzik, and J. L. O’Brien, “A variational eigenvalue solver on a photonic quantum processor,” *Nature Communications* **5**, 4213 (2014), arXiv:1304.3061 [quant-ph].
- [12] P. J. J. O’Malley, R. Babbush, I. D. Kivlichan, J. Romero, J. R. McClean, R. Barends, J. Kelly, P. Roushan, A. Tranter, N. Ding, B. Campbell, Y. Chen, Z. Chen, B. Chiaro, A. Dunsworth, A. G. Fowler, E. Jeffrey, E. Lucero, A. Megrant, J. Y. Mutus, M. Neeley, C. Neill, C. Quintana, D. Sank, A. Vainsencher, J. Wenner, T. C. White, P. V. Coveney, P. J. Love, H. Neven, A. Aspuru-Guzik, and J. M. Martinis, “Scalable quantum simulation of molecular energies,” *Phys. Rev. X* **6**, 031007 (2016).
- [13] A. Kandala, A. Mezzacapo, K. Temme, M. Takita, M. Brink, J. M. Chow, and J. M. Gambetta, “Hardware-efficient variational quantum eigensolver for small molecules and quantum magnets,” *Nature (London)* **549**, 242–246 (2017), arXiv:1704.05018 [quant-ph].
- [14] A. Aspuru-Guzik, A. D. Dutoi, P. J. Love, and M. Head-Gordon, “Simulated Quantum Computation of Molecular Energies,” *Science* **309**, 1704–1707 (2005), quant-ph/0604193.
- [15] J. R. McClean, J. Romero, R. Babbush, and A. Aspuru-Guzik, “The theory of variational hybrid quantum-classical algorithms,” *New J. Phys.* **18**, 023023 (2016), arXiv:1509.04279 [quant-ph].
- [16] R. S. Smith, M. J. Curtis, and W. J. Zeng, “A Practical Quantum Instruction Set Architecture,” (2016), arXiv:1608.03355 [quant-ph].
- [17] A. J. McCaskey, E. F. Dumitrescu, D. Liakh, M. Chen, W.-C. Feng, and T. S. Humble, “Extreme-Scale Programming Model for Quantum Acceleration within High Performance Computing,” *ArXiv e-prints* (2017), arXiv:1710.01794 [quant-ph].
- [18] A. W. Cross, L. S. Bishop, J. A. Smolin, and J. M. Gambetta, “Open Quantum Assembly Language,” *ArXiv e-prints* (2017), arXiv:1707.03429 [quant-ph].
- [19] J. R. McClean, I. D. Kivlichan, D. S. Steiger, K. J. Sung, Y. Cao, C. Dai, E. Schuyler Fried, C. Gidney, T. Häner, V. Havlíček, C. Huang, Z. Jiang, M. Neeley, J. Romero, N. Rubin, N. P. D. Sawaya, K. Setia, S. Sim, W. Sun, F. Zhang, and R. Babbush, “OpenFermion: The Electronic Structure Package for Quantum Computers,” *ArXiv e-prints* (2017), arXiv:1710.07629 [quant-ph].
- [20] J. S. Otterbach, R. Manenti, N. Alidoust, A. Bestwick, M. Block, B. Bloom, S. Caldwell, N. Didier, E. Schuyler Fried, S. Hong, P. Karalekas, C. B. Osborn, A. Pappageorge, E. C. Peterson, G. Prawiroatmodjo, N. Rubin, C. A. Ryan, D. Scarabelli, M. Scheer, E. A. Sete, P. Sivarajah, R. S. Smith, A. Staley, N. Tezak, W. J. Zeng, A. Hudson, B. R. Johnson, M. Reagor, M. P. da Silva, and C. Rigetti, “Unsupervised Machine Learning on a Hybrid Quantum Computer,” *ArXiv e-prints* (2017), arXiv:1712.05771 [quant-ph].
- [21] Yangchao Shen, Xiang Zhang, Shuaining Zhang, Jing-Ning Zhang, Man-Hong Yung, and Kihwan Kim, “Quantum implementation of the unitary coupled cluster for simulating molecular electronic structure,” *Phys. Rev. A* **95**, 020501 (2017).
- [22] U. Van Kolck, “Effective field theory of nuclear forces,” *Prog. Part. Nucl. Phys.* **43**, 337 – 418 (1999).
- [23] P. F. Bedaque and U. van Kolck, “Effective field theory for few-nucleon systems,” *Annual Review of Nuclear and Particle Science* **52**, 339–396 (2002).
- [24] S. Binder, A. Ekström, G. Hagen, T. Papenbrock, and

- K. A. Wendt, “Effective field theory in the harmonic oscillator basis,” *Phys. Rev. C* **93**, 044332 (2016).
- [25] A. Bansal, S. Binder, A. Ekström, G. Hagen, G. R. Jansen, and T. Papenbrock, “Pion-less effective field theory for atomic nuclei and lattice nuclei,” *ArXiv e-prints* (2017), arXiv:1712.10246 [nucl-th].
- [26] S. König, S. K. Bogner, R. J. Furnstahl, S. N. More, and T. Papenbrock, “Ultraviolet extrapolations in finite oscillator bases,” *Phys. Rev. C* **90**, 064007 (2014).
- [27] M. Lüscher, “Volume Dependence of the Energy Spectrum in Massive Quantum Field Theories. 1. Stable Particle States,” *Commun. Math. Phys.* **104**, 177 (1986).
- [28] R. J. Furnstahl, S. N. More, and T. Papenbrock, “Systematic expansion for infrared oscillator basis extrapolations,” *Phys. Rev. C* **89**, 044301 (2014).
- [29] S. N. More, A. Ekström, R. J. Furnstahl, G. Hagen, and T. Papenbrock, “Universal properties of infrared oscillator basis extrapolations,” *Phys. Rev. C* **87**, 044326 (2013).
- [30] Ying Li and Simon C. Benjamin, “Efficient variational quantum simulator incorporating active error minimization,” *Phys. Rev. X* **7**, 021050 (2017).
- [31] J. D. Hunter, “Matplotlib: A 2d graphics environment,” *Computing In Science & Engineering* **9**, 90–95 (2007).